

Hydrogen Peroxide Synthesis via Electrocatalytic Water Oxidation on sp^3 and sp^2 Carbon Materials Mediated by Carbonates and Bicarbonates

Wenlong Guo, Shanshan Wang, Yinqiong Xie, Chao Fang,* Lingling Liu, Qing Lou,* Xin Lian,* and Graeme Henkelman



Cite This: *ACS Sustainable Chem. Eng.* 2023, 11, 12114–12122



Read Online

ACCESS |

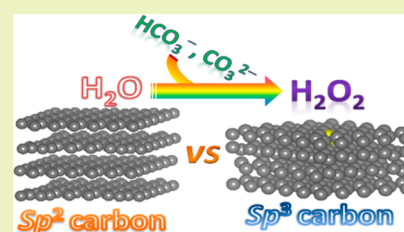
Metrics & More

Article Recommendations

Supporting Information

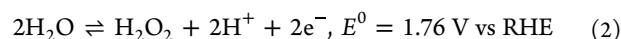
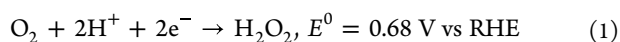
ABSTRACT: H_2O_2 production on two typical sp^3 and sp^2 carbon materials [boron-doped diamond (BDD) and graphite] via the electrochemical two-electron water oxidation reaction ($2e^-$ WOR) mediated by carbonates and bicarbonates was measured and compared. The results show that BDD exhibits superior selectivity toward the $2e^-$ WOR compared to graphite in both $KHCO_3$ and K_2CO_3 aqueous solutions. The highest Faraday efficiency (FE) for BDD in $KHCO_3$ is $\sim 20.1\%$ for 15 min of chronoamperometry measurement among all the potentials tested, while for graphite, it is $\sim 5.9\%$. Similarly, BDD achieves a maximum FE of $\sim 41.2\%$ in K_2CO_3 , while the highest FE of graphite is only $\sim 10.2\%$. Carbonate is more beneficial to the generation of H_2O_2 than bicarbonate for both BDD and graphite. Infrared spectroscopy analysis discovered that the adsorption of carbonate on the catalyst is stronger than that of bicarbonate, and the adsorption of carbonate increases with potential, while that of bicarbonate does not. Density functional theory calculations verify the stronger adsorption of carbonate on BDD and graphite than that of bicarbonate and suggest that the competitive adsorption of carbonates, bicarbonates, water, and hydroxide ions on the surface of catalysts probably essentially affects the performance of H_2O_2 production.

KEYWORDS: boron-doped diamond, carbonates and bicarbonates, graphite, hydrogen peroxide, water oxidation



INTRODUCTION

Hydrogen peroxide (H_2O_2) is an important chemical, widely used in chemical synthesis, pulp bleaching, water treatment, and the textile industry.^{1–3} Compared with the traditional anthraquinone method, electrochemical synthesis of H_2O_2 has the advantages of a simple synthesis process, nontoxic byproducts, in situ synthesis, and direct utilization, especially the electric energy can be provided by photovoltaic devices.⁴ There are two types of electrochemical synthesis of H_2O_2 , namely, cathodic two-electron oxygen reduction reaction ($2e^-$ ORR, eq 1) and anodic two-electron water oxidation reaction ($2e^-$ WOR, eq 2). H_2O_2 synthesis via the $2e^-$ ORR has been extensively researched in recent years.^{5–7} Pure aqueous H_2O_2 solutions up to 20% have been achieved using a solid electrolyte via the electrochemical $2e^-$ ORR.⁷ However, the drawbacks of this approach are that it requires a constant supply of oxygen gas and sacrifices the other reduction product on the cathode, hydrogen, a green energy source with high energy density. Compared to the $2e^-$ ORR, the technique through the $2e^-$ WOR can obtain H_2O_2 solely from water.^{8–11} Furthermore, the overall efficiency of electrochemical H_2O_2 production can be improved by forming a series electrolytic cell with anodic $2e^-$ WOR and cathodic $2e^-$ ORR.¹²

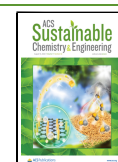


Metal oxides and carbon materials are the main anode materials for producing H_2O_2 via the $2e^-$ WOR. Generally, a suitable anode material for the $2e^-$ WOR should have some prerequisite properties, including good stability under the high oxidation potential in aqueous solution, excellent electrical conductivity, and sluggish kinetics for oxygen evolution reaction.^{12,13} A variety of metal oxides have been developed for H_2O_2 generation via the $2e^-$ WOR owing to their excellent stability under the oxidation conditions, for instance, TiO_2 ,^{14,15} SnO_2 ,^{14,16} Sb_2O_3 ,^{17,18} ZnO ,¹⁹ $BiVO_4$,^{14,20,21} $CaSnO_3$,²² $CuWO_4$,²³ and $LaAlO_3$.¹³ However, due to the poor conductivity of oxides, the reaction current density is relatively low, which leads to an unsatisfactory production rate of H_2O_2 .^{2,17} Carbon materials generally possess relatively high electrical conductivity and exhibit acceptable activity, selectivity, and stability for electrochemical H_2O_2 synthesis though the

Received: May 22, 2023

Revised: July 18, 2023

Published: August 3, 2023



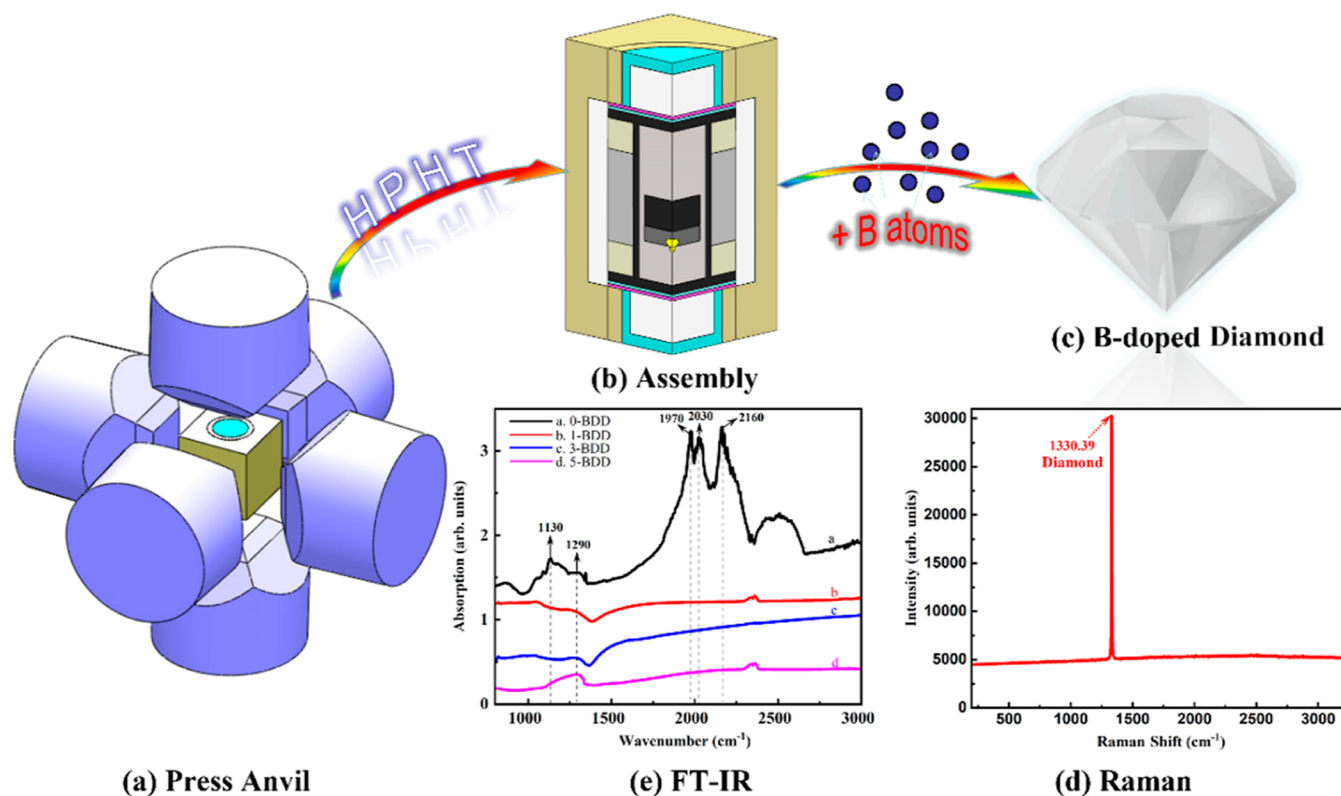


Figure 1. (a–c) Schematic diagram of the press anvil, sample assembly, and crystal cutting in the synthesis of BDD. (d) Raman spectrum of the 0-BDD sample. (e) FT-IR spectra of the 0-BDD, 1-BDD, 3BDD, and 5-BDD samples.

$2e^-$ WOR.^{22,24–33} Mavrikis and coworkers systematically investigated the electrocatalytic production of H_2O_2 by boron-doped diamond (BDD) electrodes in bicarbonate- or carbonate-based aqueous electrolytes.^{24–26} In fact, BDD has been used as the anode to electrooxidize sulfuric acid to produce peroxodisulfuric acid which further hydrolyzes to produce H_2O_2 .³⁴ Commercial carbon materials such as carbon fiber paper, carbon felt, carbon cloth, glassy carbon, and carbon gas diffusion layers have been utilized as anodes for H_2O_2 synthesis through the $2e^-$ WOR.^{28,30,33} Yang's research group used graphite electrodes for electrocatalytic production of H_2O_2 and realized that the anode produced H_2O_2 , while the cathode produced hydrogen simultaneously.²⁹ In addition, researchers have used a carbon fiber material as a substrate coated with metal oxides for electrocatalytic production of H_2O_2 .^{22,32}

It is worth noting that these carbon materials show significantly different selectivities for the $2e^-$ WOR.^{26,28,29} Selectivity is one of the important indexes to evaluate the performance of catalysts, which is closely related to the atomic arrangement, charge distribution, and adsorption of initial and intermediate species on the catalyst surface.⁹ It is well known that there are different hybrid types of carbon materials. Specifically, the hybrid type of carbon in diamond is mainly sp^3 , graphite is dominated by sp^2 carbon, and carbon fiber paper is generally a mixture of sp^2 and sp^3 carbon.³⁵ Therefore, it is necessary to explore the mechanism for the difference in selectivity between sp^2 and sp^3 carbon materials for electrocatalytic H_2O_2 production.

In addition to the intrinsic properties of catalysts, the composition of the electrolyte also plays a key role in the selectivity of H_2O_2 generation.^{36,37} Most electrocatalysts

demonstrate a higher Faraday efficiency (FE) and production rate of H_2O_2 in carbonate- and bicarbonate-based electrolytes than those in other solutions.^{18–24,29–31} It is generally accepted that these two anions act as catalytic mediums in the formation of H_2O_2 through the $2e^-$ WOR and that carbonates and bicarbonates are first oxidized to percarbonate species (HCO_4^- and $C_2O_6^{2-}$) and then hydrolyzed to H_2O_2 .^{12,28,36,38} Zheng's group confirmed the role of bicarbonate ions as a medium in electrocatalytic H_2O_2 synthesis for bismuth vanadate by using a rotating ring disk and spectroscopic experiments.³⁶ Mavrikis et al. found that the electrolyte dominated by carbonate ions is more conducive to the electrochemical generation of H_2O_2 than the solution dominated by bicarbonate ions for BDD electrodes.²⁷ Gill et al. investigated the effects of the ion concentration and molar fraction of bicarbonate and carbonate ions on the activity and selectivity of metal oxides for electrocatalytic H_2O_2 production.³⁹ Despite these efforts, the mechanism of the formation of H_2O_2 mediated by bicarbonate and carbonate needs to be further elucidated. Particularly, the mechanism for the phenomenon that the electrolyte with carbonate as the main component can promote the formation of H_2O_2 more than the electrolyte with bicarbonate as the main component is ambiguous.^{28,29} Moreover, the relationship between the adsorption of carbonates and bicarbonates on the catalyst surface and the mechanism of the catalytic performance is still not clear.

In this work, two conventional sp^3 and sp^2 carbon materials, namely, BDD and graphite, are selected as anodes to explore the performance and reaction mechanism of electrocatalytic H_2O_2 production in carbonate-based and bicarbonate-based electrolytes. In order to better reflect the intrinsic properties of the material, we synthesized diamond single crystals with

different boron impurity concentrations and chose commercial graphite sheets as electrodes for electrochemical measurements. The H₂O₂ generation performances of these two materials in potassium bicarbonate (KHCO₃) and potassium carbonate (K₂CO₃) aqueous solutions were tested. The adsorption properties of carbonates and bicarbonates on the surface of the catalysts were investigated by infrared (IR) spectroscopy and density functional theory (DFT) calculations. Our work explores the differences in the catalytic properties of sp³ and sp² carbon materials and deepens our understanding of the H₂O₂ generation mechanism mediated by carbonates and bicarbonates.

EXPERIMENTAL SECTION

Material Synthesis and Characterization. Graphite sheets (99.99%) were obtained from commercial sources and used without further treatment. The diamonds used in this work were BDD large single crystals grown by the high-pressure and high-temperature (HPHT) method. The BDDs were grown in a metallic catalyst (FeNi alloy) system with boron powder addition (purity 99.9%) under HPHT conditions using a China-type large-volume cubic high-pressure apparatus (CHPA, SPD-6×1400). The synthesis conditions were as follows: pressures ~5.6 GPa, temperatures from 1350–1400 °C, and synthesis time 40–70 h. The schematic diagram of the press anvil is shown in Figure 1a. The sample assembly is shown in Figure 1b. After the experiment, the residual solvent in the samples was removed with diluted HNO₃ (H₂O and HNO₃ 3:1, v/v), and the graphite was removed from the surface of the crystals by a hot mixed solution of H₂SO₄ and HNO₃ (3:1, v/v).^{40–42} The detailed growth assembly used in this work has been described in our previous work.⁴² Then, the samples were cut to obtain the required crystal shape (Figure 1c). The crystalline phases of synthetic diamonds were characterized by Raman spectroscopy (Figure 1d) and Fourier-transform infrared (FT-IR) spectroscopy (Figure 1e). FT-IR spectroscopy was also used to detect the adsorbed species on the catalyst surface. The added amount of boron during the synthesis of BDD is 0, 1, 3, and 5 wt %, and these samples are denoted as 0-BDD, 1-BDD, 3-BDD, and 5-BDD, respectively. Optical images of as-synthesized BDD crystals are shown in Figure S2. Obviously, as the boron addition increases, the color of the crystal gradually darkens. FT-IR spectra of BDD samples with different added amounts of boron are shown in Figure 1e. For 0-BDD, it is a typical IR spectrum of Ib-type diamond synthesized under HPHT. When boron is not added, the IR spectrum exhibits obvious diamond characteristic peaks located at 1970, 2030, and 2160 cm⁻¹. Meanwhile, there are strong absorption peaks around 1130 cm⁻¹, which are the characteristics of C-centre nitrogen in diamond (isolated substitutional nitrogen atoms). With the introduction of boron impurities, for 1-BDD, 3-BDD, and 5-BDD, only a peak at 1290 cm⁻¹ that was gradually becoming stronger was present, which corresponded to a single phonon absorption peak of boron impurity in diamond.^{40,42,43}

We compared the Raman spectra of diamond and graphite (Figure S3). The lattice of diamond is a tetrahedral structure, and the carbon atoms in the lattice are combined with each other by sp³ bonds, so the Raman characteristic peak of diamond appears at 1330 cm⁻¹.⁴⁴ The carbon atoms in the lattice of the graphite phase are bonded by sp² bonds. The crystalline graphite has two typical Raman characteristics, namely, the G peak at around 1580 cm⁻¹ and the G' peak at about 2718 cm⁻¹. The amorphous carbon components of the sp² phase are generally located in the scattering broadband of 1350–1600 cm⁻¹, and the defect D peak is about 1350 cm⁻¹, and the D' peak is about 1620 cm⁻¹.⁴⁵

Electrochemical Testing and H₂O₂ Concentration Analysis.

A CHI 760E workstation was used to conduct electrochemical tests. An H-type electrolytic cell separated with a Nafion ion exchange membrane was used for electrocatalytic reactions. A Pt sheet was used as the counter electrode, Ag/AgCl (in saturated KCl) was used as the reference electrode, and BDD or a graphite sheet was used as the

working electrode. The reaction area of the working electrode was 0.2 cm². 2 M KHCO₃ and 2 M K₂CO₃ aqueous solutions were used as the electrolytes, with pH values of 8.3 and 12, respectively. The solution volume of the anode electrolytic cell was 30 mL. A schematic diagram of the electrochemical cell used in this work is shown in Figure S4. Potentials versus the reversible H₂ electrode (RHE) were calculated by eq 3.

$$E_{\text{RHE}} = E_{\text{Ag/AgCl}} + 0.0591 \times \text{pH} + E_{\text{Ag/AgCl}}^0 (0.197 \text{ V}) \quad (3)$$

Standard test strips and the TiOSO₄ UV–vis spectrometer method were used to measure the H₂O₂ concentration in the reaction solution. Briefly, 0.01 M titanooxysulfate-sulfuric acid hydrate was dissolved in 3 M H₂SO₄. This solution was heated in a water bath and stirred until completely dissolved. We took 1 mL of the above solution and then took 1 mL of the solution from the reaction tank. We mixed these two solutions thoroughly and let them sit for 10 min. Subsequently, the absorbance of the solution at 407 nm was measured by UV–vis spectroscopy. The concentration of H₂O₂ was calculated by the change in absorbance. The FE value for H₂O₂ generation was calculated by eq 4.

$$\text{FE}(\text{H}_2\text{O}_2) = \frac{2 \times [\text{H}_2\text{O}_2] \times V \div M(\text{H}_2\text{O}_2) \times N_{\text{A}} \times 10^6}{Q \times 6.24 \times 10^{18}} \times 100\% \quad (4)$$

where FE(H₂O₂) is the FE for H₂O₂ formation, [H₂O₂] is the H₂O₂ concentration (mg/L), V is the volume of the electrolyte (mL), M(H₂O₂) is the molar mass of H₂O₂, Q is the amount of passed charge (coulomb), and N_A is the Avogadro constant.

The consumption of H₂O₂ by anodic oxidation was calculated by eq 5.

$$[\text{H}_2\text{O}_2]_{\text{anodic oxidation}} = ([\text{H}_2\text{O}_2]_{\text{added}} + [\text{H}_2\text{O}_2]_{\text{only KHCO}_3}) - [\text{H}_2\text{O}_2]_{\text{KHCO}_3 + \text{H}_2\text{O}_2} \quad (5)$$

where [H₂O₂]_{anodic oxidation} is the consumption amount of H₂O₂ by anodic oxidation, [H₂O₂]_{added} is the amount of H₂O₂ added to the electrolyte before the reaction, [H₂O₂]_{only KHCO₃} is the H₂O₂ yield tested in the KHCO₃ solution without the added H₂O₂, and [H₂O₂]_{KHCO₃ + H₂O₂} is the H₂O₂ yield tested in the KHCO₃ solution with the added H₂O₂. The calculation in K₂CO₃ is the same as in KHCO₃. [H₂O₂]_{added} + [H₂O₂]_{only KHCO₃} is the theoretical H₂O₂ production. [H₂O₂]_{KHCO₃ + H₂O₂} is the actual H₂O₂ production. The effect of anodic oxidation is described by eq 6.

$$\eta_{\text{anodic oxidation}} = \left(\frac{([\text{H}_2\text{O}_2]_{\text{theoretical}} - [\text{H}_2\text{O}_2]_{\text{actual}})}{[\text{H}_2\text{O}_2]_{\text{theoretical}}} \right) \times 100\% \quad (6)$$

RESULTS AND DISCUSSION

First, we compared the H₂O₂ production performances of BDD samples with different boron additions in KHCO₃ and K₂CO₃ aqueous solutions at various applied potentials for different testing times. The FE and production rates for the H₂O₂ synthesis of the 0-BDD, 1-BDD, 3-BDD, and 5-BDD samples are shown in Figures S6–S9. Through comprehensive comparison, 5-BDD shows relatively better electrochemical performance of H₂O₂ generation than other samples. Therefore, 5-BDD is chosen as the representative for comparative study with graphite. 5-BDD is represented by BDD throughout the following sections.

Previous studies have investigated the effect of different concentrations of KHCO₃ and K₂CO₃ on the electrocatalytic production of H₂O₂ by carbon-based materials and metal oxides.^{27,29,36} In general, the FE and production rate of H₂O₂ will gradually increase as the electrolyte concentration increases. Therefore, in this work, 2 M KHCO₃ and K₂CO₃

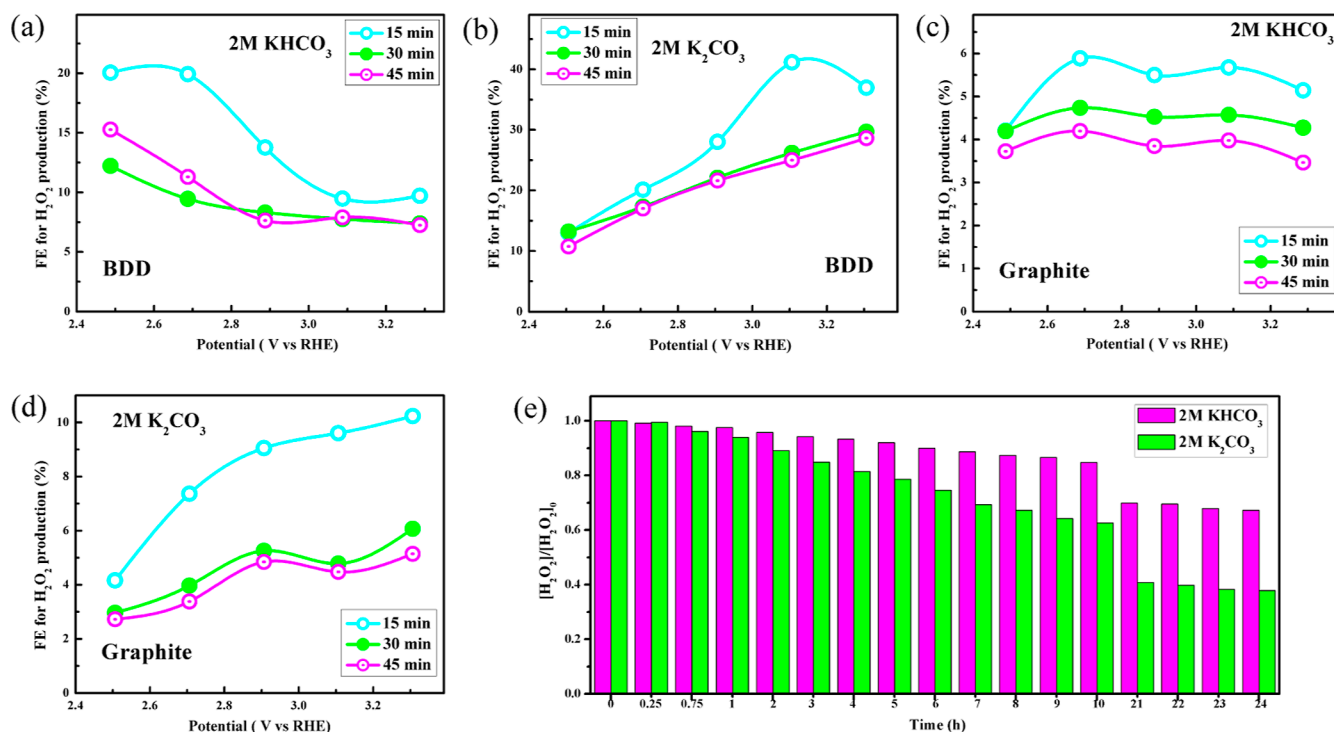


Figure 2. (a–d) FE for H₂O₂ production on BDD and graphite measured in 2 M KHCO₃ and K₂CO₃ at different potentials for various times. (e) Change in H₂O₂ concentration in KHCO₃ and K₂CO₃ as a function of time.

solutions are selected as the electrolytes for comparative study. In 2 M K₂CO₃ and KHCO₃, carbonate and bicarbonate ions dominate, respectively, according to their equilibrium mole fractions (Figure S5).³⁶ H₂O₂ FE values of BDD and graphite in 2 M K₂CO₃ and KHCO₃ solutions are shown in Figure 2a–d. Notably, higher FE values are obtained from BDD as compared to graphite in both K₂CO₃ and KHCO₃ electrolytes. In KHCO₃, the peak FE value reaches ~20.1% for BDD at 2.48 V vs RHE after a 15 min chronoamperometry test. The highest obtained FE for graphite in KHCO₃ is ~5.9% at 2.68 V vs RHE. In K₂CO₃, BDD achieves the highest FE of 41.2% at 3.10 V vs RHE, while the peak FE for graphite is 10.2% at 3.30 V vs RHE (Table S2). For both BDD and graphite, FE generally decreases as the test time increases, which has been observed in previous works,^{17,20} likely because H₂O₂ generation is accompanied by anodic oxidation and natural decomposition.³⁶ With increasing electrochemical time, more H₂O₂ is generated and accumulated in the solution, resulting in more H₂O₂ being oxidized and decomposed. In KHCO₃ and K₂CO₃, a similar trend of FE for BDD and graphite is seen as the potential gradually increases. In K₂CO₃, the FE for both BDD and graphite increases gradually as the potential increases. The FE in KHCO₃ does not increase, and it even decreases with an increase in applied potential, especially for BDD. The FE values for both BDD and graphite in K₂CO₃ at relatively positive potentials are considerably higher than those in KHCO₃, while the FE values in these two solutions are similar at lower potentials. This FE trend was also seen in a previous work of Wang's group when they tested the H₂O₂ FE of fluoride-doped tin oxide conductive glass in Na₂CO₃ and NaHCO₃ solutions.¹²

Our electrochemical tests indicate that BDD exhibits the superior selectivity of the 2e⁻WOR compared to graphite, that the carbonate-mediated electrolysis is more conducive to the

generation of H₂O₂ than the bicarbonate-mediated one (this phenomenon has been observed for BDD thin film electrodes by Mavrikis et al.²⁷), and that the FE for H₂O₂ production in KHCO₃ and K₂CO₃ has a markedly different trend with a change of applied bias. To explore the reasons for these results, we first considered the effects of decomposition and anodic oxidation on the production of H₂O₂. Figure 2e shows the variation of H₂O₂ concentrations in KHCO₃ and K₂CO₃ as a function of storage time. H₂O₂ decomposes gradually with time in both solutions, and the reduction of the H₂O₂ concentration in K₂CO₃ is more significant than that in the KHCO₃ solution. It has been reported that the stability of H₂O₂ in alkaline solution is relatively poor.^{46,47} In spite of this, the concentration of H₂O₂ in these two solutions changes very little within 1 h. After 1 hour, the amount of H₂O₂ decreased by 2.4% in KHCO₃, and this value was 5.9% in K₂CO₃. In this work, the sampling time of the reaction solution was 15, 30, and 45 min, respectively. Therefore, the natural decomposition has negligible influence on the measurement and comparison of the H₂O₂ concentration in this work. In practice, the loss of H₂O₂ caused by natural decomposition can be avoided to a large extent by in situ direct utilization (pollutant degradation) or formation of sodium percarbonate.^{12,29,30} Adding a stabilizer, such as sodium silicate, is an effective means to improve the stability of H₂O₂ in solution.²⁸ In addition to natural decomposition, anodic oxidation is also an inhibiting factor for H₂O₂ accumulation because the thermodynamic oxidation potential of H₂O₂ is only 0.68 V vs RHE.²⁷ To evaluate the effects of anodic oxidation, the H₂O₂ production on BDD and graphite after a reaction time of 15 min at different potentials in KHCO₃ and K₂CO₃ solutions with or without the addition of H₂O₂ was tested and compared (Figure 3). For graphite, the actual H₂O₂ production in KHCO₃ and K₂CO₃ electrolytes with the addition of H₂O₂ is obviously

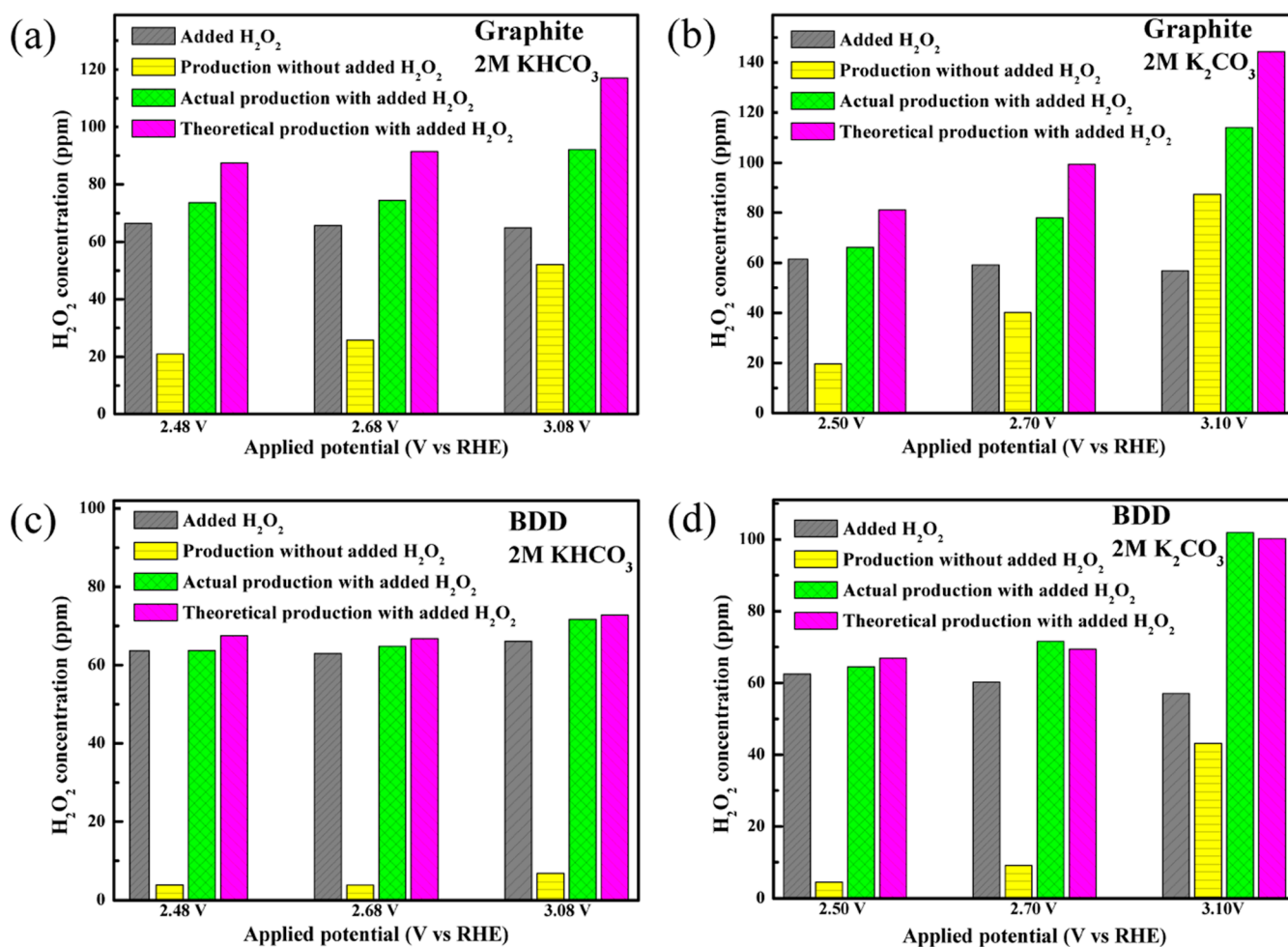


Figure 3. H₂O₂ production on graphite and BDD after chronoamperometry for 15 min at different potentials with or without added H₂O₂.

lower than the theoretical H₂O₂ production tested at different potentials. The value of $\eta_{\text{anodic oxidation}}$ for graphite in KHCO₃ tested at 2.48, 2.68, and 3.08 V vs RHE is 15.8, 18.6, and 21.3%, respectively. In K₂CO₃, for graphite, the value is 18.4, 21.5, and 20.9%, respectively. Compared to graphite, $\eta_{\text{anodic oxidation}}$ in KHCO₃ for BDD is 5.6, 2.9, and 1.6% measured at 2.48, 2.68, and 3.08 V vs RHE, respectively. In K₂CO₃, for BDD, the value is 3.6, -3.1, and -1.7%, respectively. These results suggest that the anodization of H₂O₂ on the graphite electrode is relatively serious. In contrast, for BDD, the H₂O₂ production is close to the theoretical H₂O₂ production for both KHCO₃ and K₂CO₃ solutions, especially at a higher applied bias. These results indicate that the anodic oxidation of H₂O₂ is inert on the BDD electrode compared to graphite.

To further explore the differences in performance, the adsorption of carbonate and bicarbonate on the catalyst surface was investigated. Previous reports have found that the FE and production rate of H₂O₂ can be significantly increased in relatively high concentrations of carbonate or bicarbonate electrolytes for various catalysts.^{12,16,29} Furthermore, H₂O₂ is derived from the hydrolysis of percarbonate species that originated from the electrochemical oxidation of carbonates and bicarbonates on the catalyst surface.^{12,36} These demonstrate that the adsorption of carbonate and bicarbonate is crucial for the generation of H₂O₂. FT-IR spectroscopy was used to detect the vibrational signals of carbonate and

bicarbonate species on the surface of BDD and graphite electrodes after a reaction time of 5 min at different potentials (Figure 4). The IR spectra of solid powders and aqueous solutions of KHCO₃ and K₂CO₃ are shown in Figure 4c,f. These data suggest that carbonate has strong absorption bands in the range of 1500–1200 cm⁻¹, corresponding to two degenerate stretching vibration peaks of the CO₃ group.^{36,40} In addition to an absorption band in those similar ranges, bicarbonate also has a distinct peak between 1740 and 1520 cm⁻¹. It is observed that KHCO₃ and K₂CO₃ aqueous solutions have vibrational peaks in both regions but with different intensities. This is due to ionization and hydrolysis in the carbonate and bicarbonate solutions.^{28,36} In comparison with bare and soaked samples, the adsorption of the carbonate and bicarbonate species is found to occur on the catalysts after the electrochemical reactions. Similar phenomena have been found in previous works.³⁶ All samples were thoroughly rinsed after treatment. In general, the adsorption of bicarbonate species on BDD and graphite is fairly weak and does not increase with an increase in potential. The adsorption of carbonate species on BDD and graphite is stronger than that of bicarbonate and significantly increases as the potential is moved positive. These vibrational spectra are in good agreement with the variation trend of FE for BDD and graphite in KHCO₃ and K₂CO₃ solutions with a change of applied bias, which confirms the proportional relationship

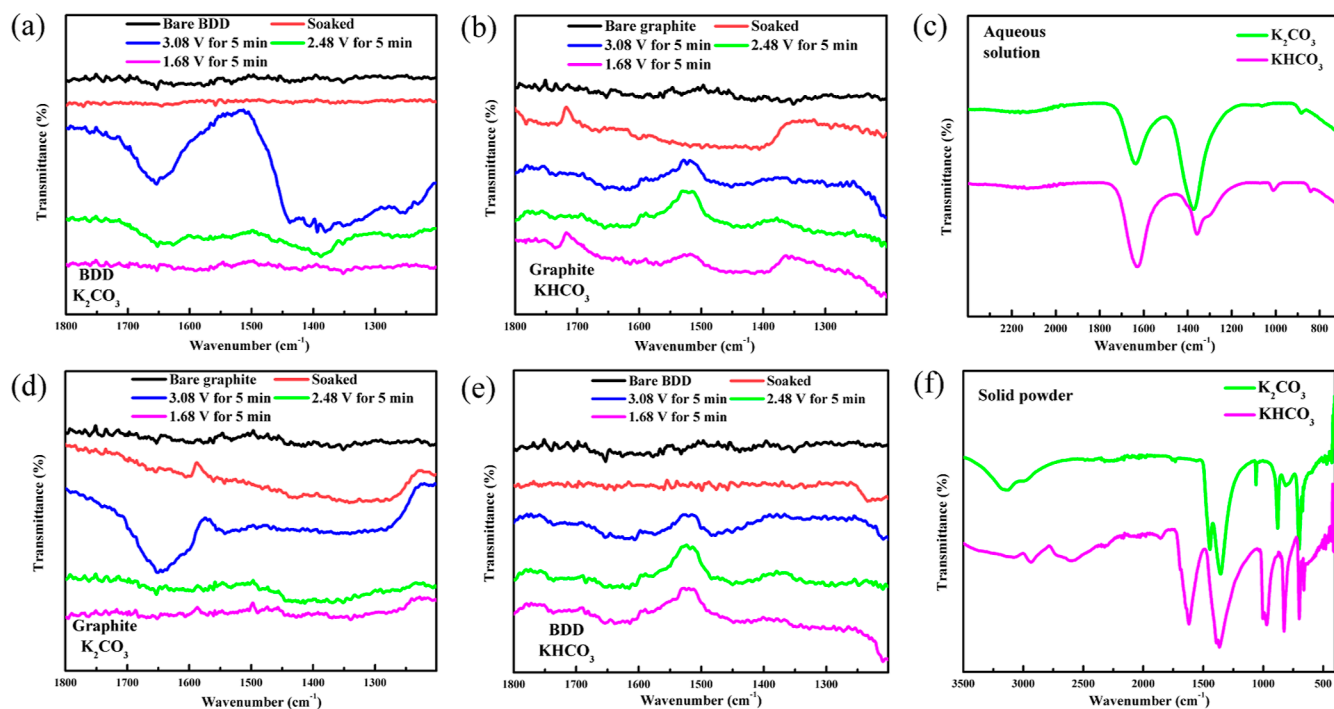


Figure 4. FT-IR spectra of bare BDD (a) and graphite (d) soaked in K_2CO_3 and in K_2CO_3 and reacted for 5 min at different potentials. FT-IR spectra of bare graphite (b) and BDD (e) soaked in $KHCO_3$ and in $KHCO_3$ and reacted for 5 min at different potentials. (c) FT-IR spectra of K_2CO_3 and $KHCO_3$ aqueous solutions. (f) FT-IR spectra of K_2CO_3 and $KHCO_3$ solid powders.

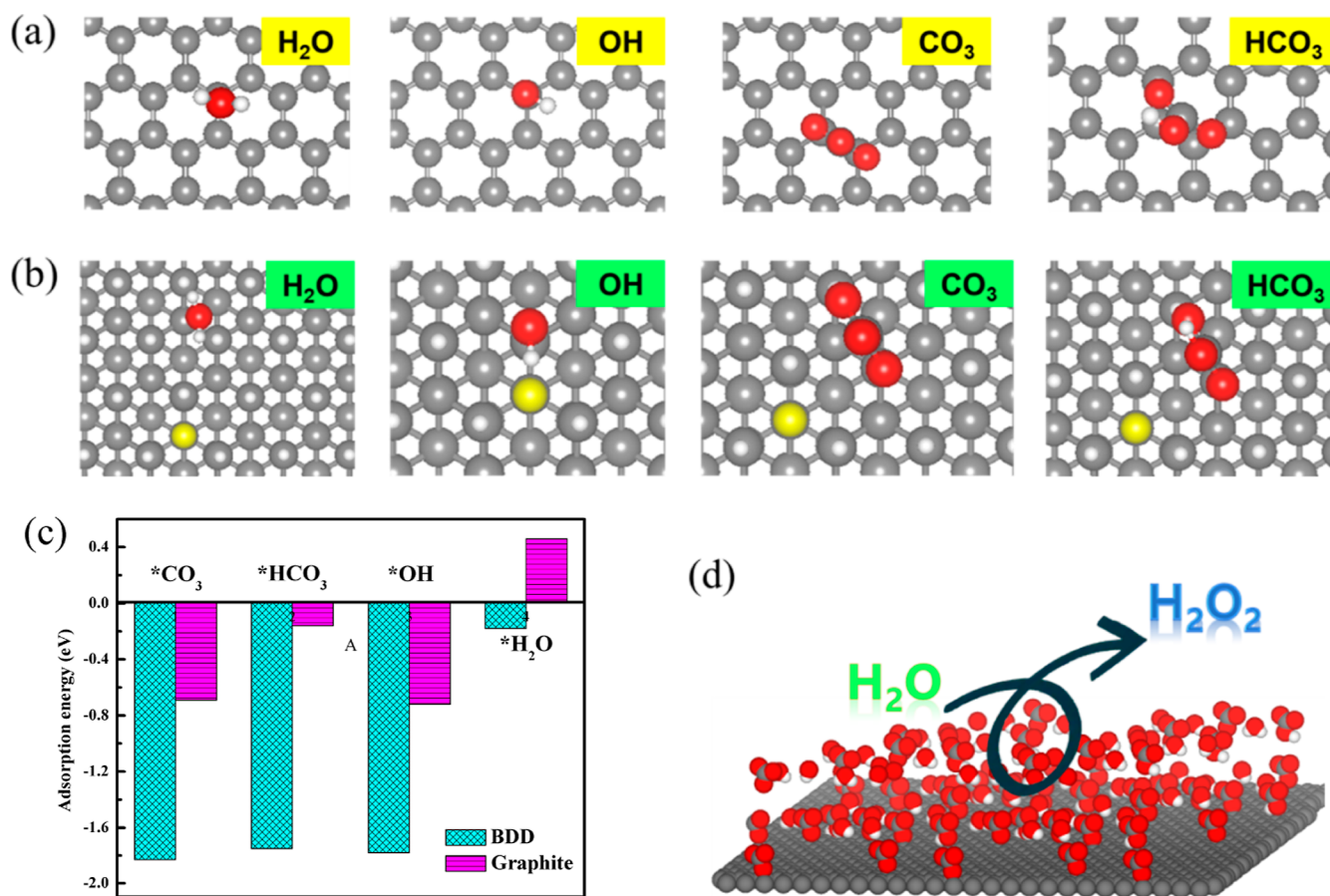


Figure 5. Structures of $*H_2O$, $*OH$, $*CO_3$, and $*HCO_3$ species adsorbed on the surfaces of (a) graphite and (b) BDD. (c) Comparison of adsorption energies of $*H_2O$, $*OH$, $*CO_3$, and $*HCO_3$ species on the surfaces of BDD and graphite. (d) Schematic diagram of electrocatalytic production of H_2O_2 mediated by carbonate and bicarbonate.

between the adsorption of carbonate and bicarbonate and the production of H_2O_2 .

In view of the importance of adsorption of carbonates and bicarbonates, DFT calculations were performed to evaluate the adsorption energies of these ions on BDD and graphite surfaces. The computational details are described in the [Supporting Information](#). In the electrochemical process, the $4e^-$ -WOR for oxygen evolution is the primary competitive reaction of the $2e^-$ -WOR for H_2O_2 production.^{12,19,21} The adsorption of water molecules and hydroxide ions on the surface of the catalyst has a fundamental effect on the $4e^-$ -WOR for oxygen evolution.^{14,48} Therefore, it is necessary to calculate and compare the adsorption of water molecules and hydroxide ions. The structures of $^*\text{H}_2\text{O}$, $^*\text{OH}$, $^*\text{CO}_3$, and $^*\text{HCO}_3$ species adsorbed on BDD and graphite are shown in [Figure 5a,b](#). These species are all adsorbed on the carbon atom through the O species. On both BDD and graphite, the adsorption energy of H_2O is rather low, especially on graphite. Under alkaline conditions, hydroxide ions will be more involved in electrochemical reactions. The strong adsorption of hydroxyl ions on the catalyst surface is likely to lead to the formation of metal-oxo species ($^*\text{O}$), which makes the catalytic reaction tend to go through the $4e^-$ -WOR process.^{48,49} Therefore, it is more suitable to estimate the reaction tendency of the $2e^-$ and $4e^-$ -WORs based on the competitive adsorption of carbonate and bicarbonate and hydroxide ions. In general, the adsorption of these ions on BDD is stronger than that on graphite, which is understandable from the different carbon hybridizations. For BDD and graphite, the adsorption energies of $^*\text{CO}_3$ species are much higher than those of HCO_3 species, which is consistent with the results of IR spectroscopy. On graphite, the adsorption energy of $^*\text{OH}$ is slightly higher than that of $^*\text{CO}_3$ but significantly higher than that of $^*\text{HCO}_3$, which is consistent with the low FE of graphite tested in the KHCO_3 solution and the relatively higher FE in the K_2CO_3 solution. On the BDD, the adsorption energy of $^*\text{CO}_3$ is higher than that of $^*\text{OH}$, and the adsorption energy of $^*\text{HCO}_3$ is marginally lower than that of $^*\text{OH}$. To some extent, these data can explain the experimental phenomenon that BDD shows higher FE in K_2CO_3 than in KHCO_3 , but both are much higher than those of graphite. As presented in [Figure 5d](#), considering the mediating effects of carbonate and bicarbonate, a stronger competitive adsorption of these ions than water and hydroxide ions in the electrocatalytic process likely results in a higher selectivity for H_2O_2 production.

CONCLUSIONS

In this work, BDD single crystals with various added amounts of boron have been synthesized, and their performance as compared to that of graphite as the anodes for electrochemical H_2O_2 production via the $2e^-$ -WOR was investigated. BDD exhibits superior selectivity for H_2O_2 generation compared to graphite in both KHCO_3 and K_2CO_3 electrolytes. For both BDD and graphite, carbonate is more beneficial to the generation of H_2O_2 than bicarbonate. In addition, the anodic oxidation of H_2O_2 is relatively sluggish on the BDD electrode compared to the graphite. In K_2CO_3 , the FE values for both BDD and graphite increase gradually as the potential increases in general, while in KHCO_3 , the FE does not increase, and it even decreases with an increase in applied potential. The IR spectra show that the adsorption of carbonate on BDD or graphite is stronger than that of bicarbonate, and the adsorption of carbonate increases with potential, while the

adsorption of bicarbonate does not. DFT calculations confirm the stronger adsorption of carbonate than that of bicarbonate on BDD and graphite, suggesting that the competitive adsorption of carbonates, bicarbonates, water, and hydroxide ions on the surface of catalysts probably fundamentally affects the selectivity of the catalyst for the $2e^-$ -WOR.

ASSOCIATED CONTENT

Supporting Information

The Supporting Information is available free of charge at <https://pubs.acs.org/doi/10.1021/acssuschemeng.3c03031>.

Computational details, characterization data, and electrochemical performances (PDF)

AUTHOR INFORMATION

Corresponding Authors

Chao Fang – Key Laboratory of Material Physics of Ministry of Education, School of Physics and Microelectronics, Zhengzhou University, Zhengzhou 450052, China; orcid.org/0000-0001-7322-1566; Email: fangchao1989@zzu.edu.cn

Qing Lou – Key Laboratory of Material Physics of Ministry of Education, School of Physics and Microelectronics, Zhengzhou University, Zhengzhou 450052, China; orcid.org/0000-0002-8852-8453; Email: louqing1986@zzu.edu.cn

Xin Lian – College of Chemistry and Chemical Engineering, Chongqing University of Science and Technology, Chongqing 401331, P. R. China; orcid.org/0000-0003-2107-0641; Email: daisylian0121@163.com

Authors

Wenlong Guo – Chongqing Key Laboratory of Green Synthesis and Applications, College of Chemistry, Chongqing Normal University, Chongqing 401331, P. R. China

Shanshan Wang – Chongqing Key Laboratory of Green Synthesis and Applications, College of Chemistry, Chongqing Normal University, Chongqing 401331, P. R. China

Yinqiong Xie – Chongqing Key Laboratory of Green Synthesis and Applications, College of Chemistry, Chongqing Normal University, Chongqing 401331, P. R. China

Lingling Liu – Chongqing Key Laboratory of Green Synthesis and Applications, College of Chemistry, Chongqing Normal University, Chongqing 401331, P. R. China

Graeme Henkelman – Department of Chemistry and the Oden Institute for Computational Engineering and Sciences, The University of Texas, Austin, Texas 78712, United States; orcid.org/0000-0002-0336-7153

Complete contact information is available at: <https://pubs.acs.org/doi/10.1021/acssuschemeng.3c03031>

Notes

The authors declare no competing financial interest.

ACKNOWLEDGMENTS

We gratefully acknowledge the Texas Advanced Computing Center for computational resources and funding from the National Natural Science Foundation of China (grant nos. 12274373, U2004168, 12074348), the Scientific and Technological Project in Henan Province, China (grant no. 222102230018), and the Chongqing Innovation Research Group Project (no. CXQT21015).

REFERENCES

- (1) Campos-Martin, J. M.; Blanco-Brieva, G.; Fierro, J. L. Hydrogen Peroxide Synthesis: an Outlook beyond the Anthraquinone Process. *Angew. Chem., Int. Ed.* **2006**, *45*, 6962–6984.
- (2) Mavrikis, S.; Perry, S. C.; Leung, P. K.; Wang, L.; Ponce de León, C. Recent Advances in Electrochemical Water Oxidation to Produce Hydrogen Peroxide: A Mechanistic Perspective. *ACS Sustainable Chem. Eng.* **2020**, *9*, 76–91.
- (3) Herman, A.; Mathias, J. L.; Neumann, R. Electrochemical Formation and Activation of Hydrogen Peroxide from Water on Fluorinated Tin Oxide for Baeyer–Villiger Oxidation Reactions. *ACS Catal.* **2022**, *12*, 4149–4155.
- (4) Sun, Y.; Han, L.; Strasser, P. A Comparative Perspective of Electrochemical and Photochemical Approaches for Catalytic H₂O₂ Production. *Chem. Soc. Rev.* **2020**, *49*, 6605–6631.
- (5) Lu, Z.; Chen, G.; Siahrostami, S.; Chen, Z.; Liu, K.; Xie, J.; Liao, L.; Wu, T.; Lin, D.; Liu, Y.; Jaramillo, T. F.; Nørskov, J. K.; Cui, Y. High-Efficiency Oxygen Reduction to Hydrogen Peroxide Catalysed by Oxidized Carbon Materials. *Nat. Catal.* **2018**, *1*, 156–162.
- (6) Kim, H. W.; Ross, M. B.; Kornienko, N.; Zhang, L.; Guo, J.; Yang, P.; McCloskey, B. D. Efficient Hydrogen Peroxide Generation using Reduced Graphene Oxide-Based Oxygen Reduction Electrocatalysts. *Nat. Catal.* **2018**, *1*, 282–290.
- (7) Xia, C.; Xia, Y.; Zhu, P.; Fan, L.; Wang, H. Direct Electrosynthesis of Pure Aqueous H₂O₂ Solutions up to 20% by Weight using a Solid Electrolyte. *Science* **2019**, *366*, 226–231.
- (8) Xue, Y.; Wang, Y.; Pan, Z.; Sayama, K. Electrochemical and Photoelectrochemical Water Oxidation for Hydrogen Peroxide Production. *Angew. Chem., Int. Ed.* **2021**, *60*, 10469–10480.
- (9) Tang, J.; Zhao, T.; Solanki, D.; Miao, X.; Zhou, W.; Hu, S. Selective Hydrogen Peroxide Conversion Tailored by Surface, Interface, and Device Engineering. *Joule* **2021**, *5*, 1432–1461.
- (10) Liu, J.; Zou, Y.; Jin, B.; Zhang, K.; Park, J. H. Hydrogen Peroxide Production from Solar Water Oxidation. *ACS Energy Lett* **2019**, *4*, 3018–3027.
- (11) Yang, S.; Verdaguier-Casadevall, A.; Arnarson, L.; Silvioli, L.; Čolić, V.; Frydendal, R.; Rossmel, J.; Chorkendorff, I.; Stephens, I. E. L. Toward the Decentralized Electrochemical Production of H₂O₂: A Focus on the Catalysis. *ACS Catal.* **2018**, *8*, 4064–4081.
- (12) Fan, L.; Bai, X.; Xia, C.; Zhang, X.; Zhao, X.; Xia, Y.; Wu, Z. Y.; Lu, Y.; Liu, Y.; Wang, H. CO₂/Carbonate-Mediated Electrochemical Water Oxidation to Hydrogen Peroxide. *Nat. Commun.* **2022**, *13*, 2668.
- (13) Baek, J.; Jin, Q.; Johnson, N. S.; Jiang, Y.; Ning, R.; Mehta, A.; Siahrostami, S.; Zheng, X. Discovery of LaAlO₃ as an Efficient Catalyst for Two-Electron Water Electrolysis towards Hydrogen Peroxide. *Nat. Commun.* **2022**, *13*, 7256.
- (14) Shi, X.; Siahrostami, S.; Li, G. L.; Zhang, Y.; Chakhranont, P.; Studt, F.; Jaramillo, T. F.; Zheng, X.; Nørskov, J. K. Understanding Activity Trends in Electrochemical Water Oxidation to Form Hydrogen Peroxide. *Nat. Commun.* **2017**, *8*, 701.
- (15) Xue, S. G.; Tang, L.; Tang, Y. K.; Li, C. X.; Li, M. L.; Zhou, J. J.; Chen, W.; Zhu, F.; Jiang, J. Selective Electrocatalytic Water Oxidation to Produce H₂O₂ Using a C,N Codoped TiO₂ Electrode in an Acidic Electrolyte. *ACS Appl. Mater. Interfaces* **2020**, *12*, 4423–4431.
- (16) Guo, W.; Xie, Y.; Tang, S.; Yu, B.; Lian, X.; Henkelman, G.; Liu, X. H₂O₂ Formation Mechanisms on the (1 1 2) and (3 1 0) Facets of SnO₂ via Water Oxidation Reaction with the Participation of Bicarbonate: DFT and Experimental Investigations. *Appl. Surf. Sci.* **2022**, *596*, 153634.
- (17) Wang, Y.; Lian, X.; Zhou, Y.; Guo, W.; He, H. Synthesis and Characterization of Sb₂O₃: a Stable Electrocatalyst for Efficient H₂O₂ Production and Accumulation and Effective Degradation of Dyes. *New J. Chem.* **2021**, *45*, 8958–8964.
- (18) Guo, W.; Xie, Y.; Liu, Y.; Shang, S.; Lian, X.; Liu, X. Effects of Sb₂O₃ Polymorphism on the Performances for Electrocatalytic H₂O₂ Production via the Two-Electron Water Oxidation Reaction. *Appl. Surf. Sci.* **2022**, *606*, 155006.
- (19) Kelly, S. R.; Shi, X.; Back, S.; Vallez, L.; Park, S. Y.; Siahrostami, S.; Zheng, X.; Nørskov, J. K. ZnO As an Active and Selective Catalyst for Electrochemical Water Oxidation to Hydrogen Peroxide. *ACS Catal.* **2019**, *9*, 4593–4599.
- (20) Nadar, A.; Gupta, S. S.; Kar, Y.; Shetty, S.; van Bavel, A. P.; Khushalani, D. Evaluating the Reactivity of BiVO₄ Surfaces for Efficient Electrocatalytic H₂O₂ Production: A Combined Experimental and Computational Study. *J. Phys. Chem. C* **2020**, *124*, 4152–4161.
- (21) Baek, J. H.; Gill, T. M.; Abroshan, H.; Park, S.; Shi, X.; Nørskov, J.; Jung, H. S.; Siahrostami, S.; Zheng, X. Selective and Efficient Gd-Doped BiVO₄ Photoanode for Two-Electron Water Oxidation to H₂O₂. *ACS Energy Lett* **2019**, *4*, 720–728.
- (22) Zhang, C.; Lu, R.; Liu, C.; Yuan, L.; Wang, J.; Zhao, Y.; Yu, C. High Yield Electrosynthesis of Hydrogen Peroxide from Water Using Electrospun CaSnO₃@Carbon Fiber Membrane Catalysts with Abundant Oxygen Vacancy. *Adv. Funct. Mater.* **2021**, *31*, 2100099.
- (23) Li, L.; Xiao, K.; Wong, P. K.; Hu, Z.; Yu, J. C. Hydrogen Peroxide Production from Water Oxidation on a CuWO₄ Anode in Oxygen-Deficient Conditions for Water Decontamination. *ACS Appl. Mater. Interfaces* **2022**, *14*, 7878–7887.
- (24) Mavrikis, S.; Göltz, M.; Rosiwal, S.; Wang, L.; Ponce de León, C. Boron-Doped Diamond Electrocatalyst for Enhanced Anodic H₂O₂ Production. *ACS Appl. Mater. Interfaces* **2020**, *3*, 3169–3173.
- (25) Wenderich, K.; Nieuweweme, B. A. M.; Mul, G.; Mei, B. T. Selective Electrochemical Oxidation of H₂O to H₂O₂ Using Boron-Doped Diamond: An Experimental and Techno-Economic Evaluation. *ACS Sustainable Chem. Eng.* **2021**, *9*, 7803–7812.
- (26) Mavrikis, S.; Göltz, M.; Perry, S. C.; Bogdan, F.; Leung, P. K.; Rosiwal, S.; Wang, L.; Ponce de León, C. Effective Hydrogen Peroxide Production from Electrochemical Water Oxidation. *ACS Energy Lett* **2021**, *6*, 2369–2377.
- (27) Mavrikis, S.; Goltz, M.; Rosiwal, S.; Wang, L.; Ponce de León, C. Carbonate-Induced Electrosynthesis of Hydrogen Peroxide via Two-Electron Water Oxidation. *ChemSusChem* **2022**, *15*, No. e202102137.
- (28) Pangotra, D.; Csepei, L.-I.; Roth, A.; Ponce de León, C.; Sieber, V.; Vieira, L. Anodic Production of Hydrogen Peroxide using Commercial Carbon Materials. *Appl. Catal. B: Environ.* **2022**, *303*, 120848.
- (29) Ye, H.; Yang, L.; Nie, X.; Liu, K.; Yang, S.; Zhou, Y.; Dong, F.; He, H.; Yang, H. Dual-functional Water Splitting: Electro-Fenton-Like Pollutants Degradation from Anode Reaction and Hydrogen Fuel Production from Cathode Reaction. *Electrochim. Acta* **2021**, *394*, 139122.
- (30) Xia, C.; Back, S.; Ringe, S.; Jiang, K.; Chen, F.; Sun, X.; Siahrostami, S.; Chan, K.; Wang, H. Confined Local Oxygen Gas Promotes Electrochemical Water Oxidation to Hydrogen Peroxide. *Nat. Catal.* **2020**, *3*, 125–134.
- (31) Sun, Y.; Chen, X.; Ning, S.; Zhou, W.; Yang, Z.; Cui, J.; Wang, D.; Ye, J.; Liu, L. Efficient Electrochemical Water Oxidation to Hydrogen Peroxide over Intrinsic Carbon Defect-Rich Carbon Nanofibers. *J. Mater. Chem. A* **2021**, *9*, 23994–24001.
- (32) Zhang, C.; Lu, J.; Liu, C.; Zou, Y.; Yuan, L.; Wang, J.; Yu, C. ZnO Nanoparticles Embedded in Hollow Carbon Fiber Membrane for Electrochemical H₂O₂ Production by Two-Electron Water Oxidation Reaction. *Environ. Res.* **2022**, *206*, 112290.
- (33) Ando, Y. Proposal for a New System for Simultaneous Production of Hydrogen and Hydrogen Peroxide by Water Electrolysis. *Int. J. Hydrogen Energy* **2004**, *29*, 1349–1354.
- (34) Serrano, K.; Michaud, P.; Comminellis, C.; Savall, A. Electrochemical Preparation of Peroxodisulfuric Acid using Boron Doped Diamond Thin Film Electrodes. *Electrochim. Acta* **2002**, *48*, 431–436.
- (35) He, X.; Zhang, F.; Wang, R.; Liu, W. Preparation of a carbon nanotube/carbon fiber multi-scale reinforcement by grafting multi-walled carbon nanotubes onto the fibers. *Carbon* **2007**, *45*, 2559–2563.

- (36) Gill, T. M.; Vallez, L.; Zheng, X. The Role of Bicarbonate-Based Electrolytes in H₂O₂ Production through Two-Electron Water Oxidation. *ACS Energy Lett* **2021**, *6*, 2854–2862.
- (37) Seitz, A. K.; Kohlpaintner, P. J.; van Lingen, T.; Dyga, M.; Sprang, F.; Zirbes, M.; Waldvogel, S. R.; Gooßen, L. J. Concentrated Aqueous Peroxodicarbonate: Efficient Electrosynthesis and Use as Oxidizer in Epoxidations, S- and N-Oxidations. *Angew. Chem., Int. Ed.* **2022**, *61*, No. e202117563.
- (38) Fuku, K.; Sayama, K. Efficient oxidative hydrogen peroxide production and accumulation in photoelectrochemical water splitting using a tungsten trioxide/bismuth vanadate photoanode. *Chem. Commun.* **2016**, *52*, 5406–5409.
- (39) Gill, T. M.; Vallez, L.; Zheng, X. Enhancing Electrochemical Water Oxidation toward H₂O₂ via Carbonaceous Electrolyte Engineering. *ACS Appl. Energ. Mater.* **2021**, *4*, 12429–12435.
- (40) Chen, L.; Miao, X.; He, X.; Guo, L.; Fang, S.; Wang, Y.; Wang, Z.; Fang, C.; Ma, H.; Jia, X. Effects of Fe-Ni solvent with different Fe contents on the boron concentration in colorless diamonds. *J. Cryst. Growth* **2018**, *498*, 67–70.
- (41) Fang, C.; Jia, X.; Chen, N.; Li, Y.; Guo, L.; Chen, L.; Ma, H.-a.; Liu, X. HPHT synthesis of N–H co-doped diamond single crystals. *J. Crystal. Growth* **2016**, *436*, 34–39.
- (42) Zhou, G.-T.; Mu, Y.-H.; Song, Y.-W.; Zhang, Z.-F.; Zhang, Y.-W.; Shen, W.-X.; Wang, Q.-Q.; Wan, B.; Fang, C.; Chen, L.-C.; Li, Y.-D.; Jia, X.-P. Synergistic influences of titanium, boron, and oxygen on large-size single-crystal diamond growth at high pressure and high temperature. *Chinese Phys. B.* **2022**, *31*, 068103.
- (43) Chrenko, R. M. Boron, the Dominant Acceptor in Semiconducting Diamond. *Phys. Rev. B* **1973**, *7*, 4560–4567.
- (44) Fang, C.; Zhang, Y.; Shen, W.; Sun, S.; Zhang, Z.; Xue, L.; Jia, X. Synthesis and characterization of HPHT large single-crystal diamonds under the simultaneous influence of oxygen and hydrogen. *Crystengcomm* **2017**, *19*, 5727–5734.
- (45) Reich, S.; Thomsen, C. Raman spectroscopy of graphite. *Phil. Trans. R. Soc. Lond. A.* **2004**, *362*, 2271–2288.
- (46) Cota, H. M. Decomposition of Dilute Hydrogen Peroxide in Alkaline Solutions. *Nature* **1964**, *203*, 1281.
- (47) Nicoll, W. D.; Smith, A. F. Stability of Dilute Alkaline Solutions of Hydrogen Peroxide. *J. Ind. and Eng. Chem.* **1955**, *47*, 2548–2554.
- (48) Siahrostami, S.; Li, G. L.; Viswanathan, V.; Norskov, J. K. One- or Two-Electron Water Oxidation, Hydroxyl Radical, or H₂O₂ Evolution. *J. Phys. Chem. Lett.* **2017**, *8*, 1157–1160.
- (49) Viswanathan, V.; Hansen, H. A.; Norskov, J. K. Selective Electrochemical Generation of Hydrogen Peroxide from Water Oxidation. *J. Phys. Chem. Lett.* **2015**, *6*, 4224–4228.